Proceedings of the Canadian Society for Mechanical Engineering International Congress 2021
CSME Congress 2021
June 27-30, 2021, Charlottetown, PE, Canada

Realistic Representative Volume Element Generation for Sintered Solids Part 2: Finite Element Implementation & Results

D. Frank Thomas*, A .Y. Elruby, Sam Nakhla
Faculty of Engineering and Applied Science (Mechanical)
Memorial University of Newfoundland
*dft135@mun.ca

Abstract—The following work presents the process by which the model generation algorithm from Part 1 is implemented in ABAQUS finite element analysis software. Convergence analysis was conducted for the elastic modulus. Simulation results are compared to experimental results for 2D and 3D models. Model performance is evaluated both in the linear elastic region and at strains of up to 10%. Stress field diagrams were captured to illustrate the unusual stress concentration patterns that are unique to powder-based sintered materials.

Keywords: microstructure modelling, porous sintered solid, finite element analysis, representative volume element

I. INTRODUCTION

The naturally occurring void imperfections observed in sintered materials are unique in both shape and size compared to the macro-scale voids observed in non-sintered solids, which are generally ellipsoidal. This shape disparity has a significant effect on the material's mechanical behavior [1]. Specifically, void shapes inherent in sintered materials facilitate compaction deformation under compressive loading thereby exacerbating the disparity between the tensile and compressive elastoplastic behavior of sintered metals [2] [3]. The accurate prediction of the mechanical properties of low porosity sintered materials is crucial to the design of powder-based components.

Investigations into the mechanical behavior of AM materials have been augmented significantly by simulation techniques developed through composite materials research, such as the representative volume element (RVE), in concert with modern finite element analysis (FEA) [4]. Microstructure modelling in particular has proven to be a powerful tool for assessing material properties. Modelling and analysis of a microstructural element can accurately predict behavior while simplifying the process of parameterization where a descriptive analytical model is desired. In the case of porous sintered materials, the microstructure has yet to be modelled in a generalized manner such that behavior is accurately predicted.

Homogenization and generalization of stress-strain behavior from microstructural simulation is made possible by the application of continuum mechanics principles. This information is sufficient to evaluate the mechanical behavior of an arbitrary shape whose material properties are known. The continuum approach introduces the assumption that the structural element may be treated as an infinitesimally small element surrounded by identical cells under identical load conditions. In addition to vastly simplifying microstructure simulations as a whole, the cost-effective simulation of infinite cells has been a powerful tool for the investigation of porous and cellular solids.

II. ABAQUS IMPLEMENTATION

A. Model Generation

The model generation module is handed a particle array and exterior/interior boundary lengths from the compaction module. The model generator begins in the part module, generating a numbered part for each particle in the array. The final part created is the external RVE shell. Moving to the assembly module, a second loop instantiates and translates each particle to the assigned coordinates. The shell component is placed in the assembly and merging is performed to produce the final RVE instance. It is at this point that material properties may be applied to the model. The default material model is an elastoplastic formulation which ABAQUS refers to as deformation plasticity.

B. Analysis Methods

Two analysis methods, elastic and elastoplastic, have been built into the script. The elastic analysis will create a linear perturbation step wherein a miniscule strain ($\varepsilon = 0.001$) is applied in a single increment over a negligible time period. The model's linear elastic stiffness is evaluated from the base state, thereby negating the effect of non-linear deformation behavior [5]. This analysis method is the most rapid and reliable way to calculate the effective elastic modulus.

The elastoplastic analysis method is intended for investigations of large-deformation behaviors in tension and compression. It uses a general static step segmented into equally

spaced intervals. The nature of compaction behavior in sintered materials requires well defined surface self-contact properties. The primary output of this analysis is a homogenized stress-strain relationship capturing both elastic and plastic deformation behavior.

C. Boundary Conditions

The boundary conditions imposed in both elastic and elastoplastic investigations include rigid top and bottom surfaces. Each node of a rigid surface is tied to a reference node at the center of the face such that these nodes cannot move with respect to the reference. A fixed condition is applied to the bottom reference point, restricting the bottom surface completely. A displacement load is generated for the top reference point such that some non-zero uniaxial displacement is applied in the Y-axis during analysis. This condition also restricts rotation of the top surface about the X- and Z-axes. Field output requests are instated to capture reaction force at the bottom reference node and displacement at the top reference node.

III. Results and Discussion

A. 2D Simulation Results – Convergence

Convergence studies were performed on low- to medium-porosity 2D specimens investigating the effect of porosity on elastic modulus. One such convergence plot is shown in Fig. 1.

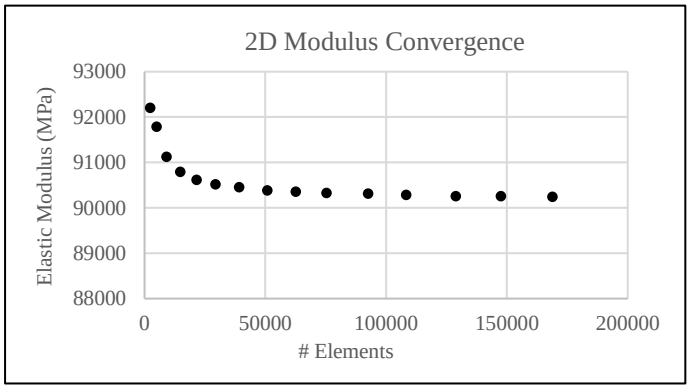

Figure 1. 2D Modulus Convergence Plot

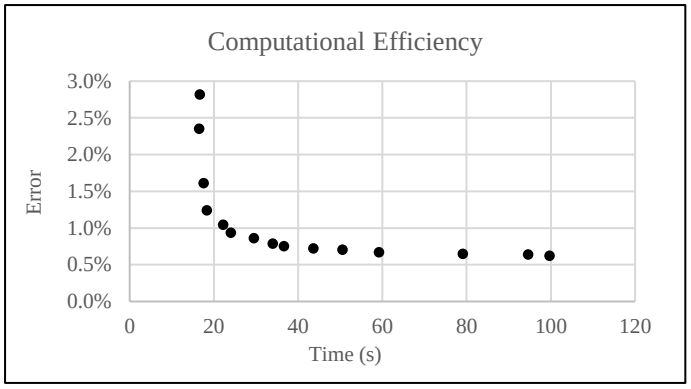

Figure 2. Computational Load vs. Accuracy

B. 2D Simulation Results - Accuracy

Simulation results for elastic modulus investigations are compared to experimental findings in Table 1. The models used in these simulations were generated with a unit length of 10 and a mean particle radius of 0.5 with a standard deviation of 0.1.

A mesh seed was defined with a maximum element length of 0.025, thus achieving a quantity of elements deemed sufficient by the convergence study. The analysis step used was linear perturbation, whereby a very small strain is applied over an arbitrarily small step time assuming linear elastic behavior [5]. We observe that the maximum percent difference in elastic modulus between experimental results and simulation results is 2.83% when comparing titanium and high-strength steel specimens having porosities in the range of 0.9% – 11.7%.

C. 3D Simulation Results – Convergence

We observe from Fig. 3 that the elastic modulus converges at approximately 300,000 elements. Lower resolution meshes are inhibited by the very small voids found in the final specimen, which require at least one seed per edge with a growth rate of 1.1 regardless of the global seed size. This growth rate refers to the maximum ratio of adjacent element side lengths in the transition zone from a high resolution to a low resolution mesh region.

D. 3D Simulation Results – Accuracy

3D simulation results for elastic modulus investigations are shown compared to experimental findings in Tables 1 & 2. The models used in these simulations were generated with a unit length of 10 and a mean particle radius of 1.0 with a standard deviation of 0.1. A mesh seed was defined with a maximum element length of 0.1, thus achieving a quantity of elements deemed sufficient by the convergence study depicted in Fig. 3. The analysis step used was a linear perturbation, as per the 2D simulations. We observe that the maximum percent difference in elastic modulus between experimental results and simulation results is 2.39%.

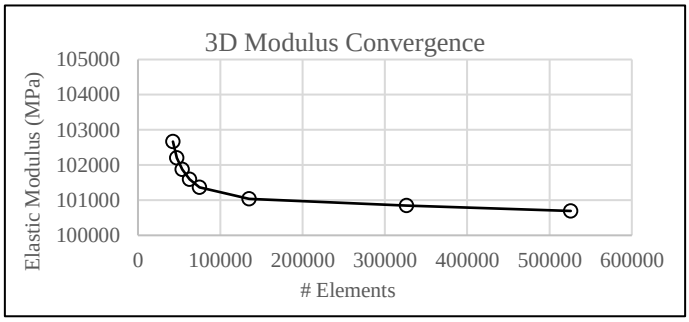

Figure 3. 3D Modulus Convergence Plot

TABLE 1: CP-TI ELASTIC RESULTS

Porosity	Elastic Modulus	Results		% Difference	
		2D	3D	2D	3D
0.0%	110.0	-	-	-	-
4.5%	95.7	95.47	97.45	0.24%	1.83%
7.8%	86.3	84.56	88.361	2.02%	2.39%

TABLE 2. HIGH-STRENGTH SINTERED STEEL ELASTIC RESULTS

Porosity	Elastic Modulus	Results		% Difference	
		2D	3D	2D	3D
0.0%	144.0	-	-	-	-
4.0%	127.2	124.56	130.17	2.08%	2.33%
7.0%	115.9	112.62	116.72	2.83%	0.71%

E. Large Deformation Simulation Results

A series of large deformation analyses were conducted on 2D and 3D specimens in the porosity range of 3.5% - 10.3%. The material properties of the experimental specimens are tabulated below. Given values for offset and hardening exponent refer to the parameters of the deformation plasticity material model which describe the plastic behavior of a fully dense specimen.

In each of the following large deformation analyses the 2D mesh is constructed of free-structured linear tri elements of type CPS3 while 3D meshes use free-structured linear tetrahedral elements type C3D4. In each case the bottom surface is fixed in place while a ramp displacement is applied to the opposite face in a static analysis step with consideration for non-linear geometry effects. A maximum increment time period is specified such that the analysis returns a minimum of 25 data points along the stress-strain curve.

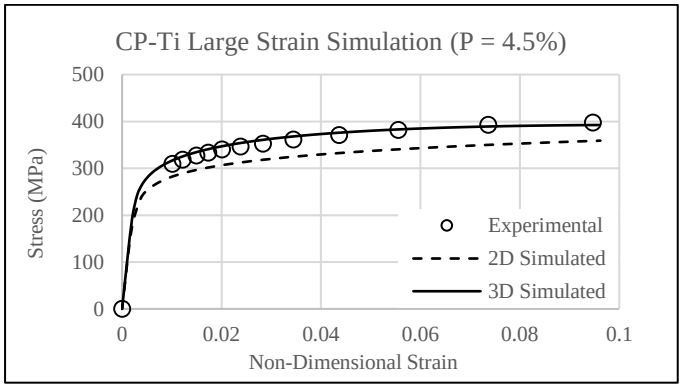

Figure 4. CP-Ti Large Deformation Plot 1

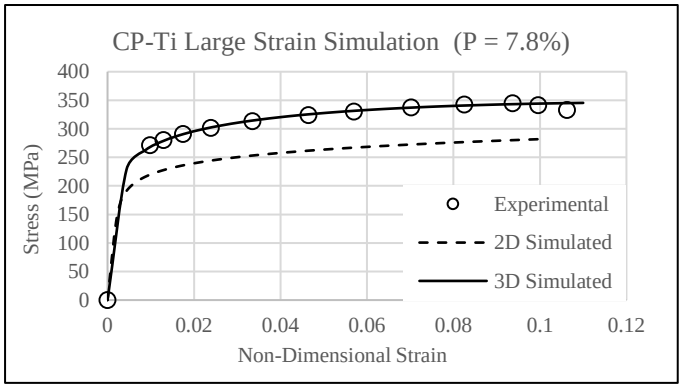

Figure 5. CP-Ti Large Deformation Plot 2

TABLE 3. LARGE DEFORMATION MATERIAL PROPERTIES

Material	**E** (GPa)	σ_y (MPa)	ν
CP-Ti	110.0	270.0	0.33
316L SS	190.0	460.0	0.25

F. CP-Ti Simulation Results

Figures 4 and 5 depict the simulated mechanical behavior of porous specimens of commercially pure titanium in comparison to physical test data from Bourcier et al. [6]. These sintered powder-fabricated specimens were loaded in uniaxial tension to failure, with each specimen having a failure strain of $\varepsilon \approx 0.1$. We observe that, in both trials, the 2D and 3D simulations accurately predict elastic modulus as anticipated. The 3D analyses produce stress-strain behavior that is highly similar to physical test data up to the ultimate tensile stress. Analysis of 2D models would appear to over-predict the effect of porosity on the tensile yield stress by ~40 MPa in the 4.5% porous study and ~60 MPa in the 7.8% porous model, a percent error of ~14% and ~25% respectively.

G. 316L Stainless Steel Simulation Results

Figures 6 and 7 depict the simulated mechanical behavior of 4.5% and 10.3% porous specimens of 316L stainless steel from Chawla and Deng [7]. Failure strains are recorded as 0.045 and 0.02 respectively. As we observed in the 4.5% porous CP-Ti comparison, this steel investigation displays an accurate prediction of the elastic properties in both 2D and 3D, under-prediction of yield stress in 2D, and a good prediction of elastoplastic behavior in 3D up to the point of failure. At a porosity of 10.3%, the 3D model analysis gives an accurate prediction of mechanical behavior throughout the elastoplastic region. The 2D model analysis in this case under predicts both the elastic modulus and the yield stress appreciably.

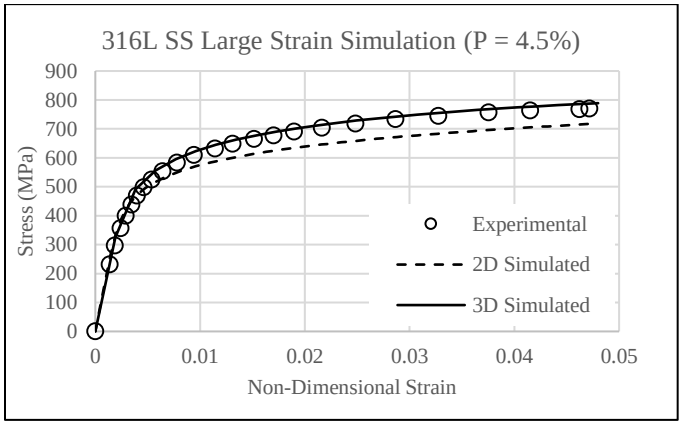

Figure 6. 316L SS Large Deformation Plot 1

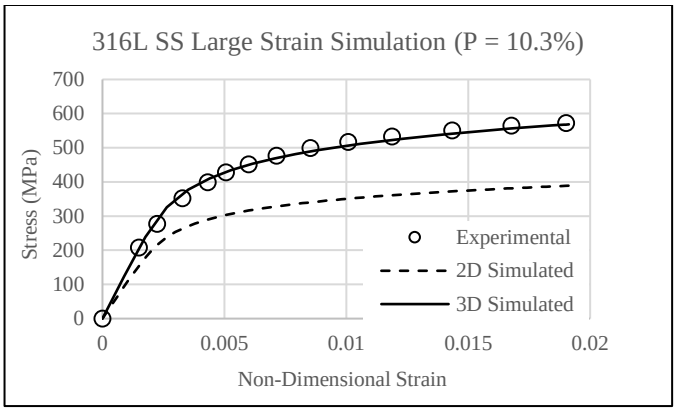

Figure 7. 316L SS Large Deformation Plot 2

IV. Stress Distribution

The stress distributions seen in figures 8 & 9 correspond to a 5% porous sample of Ti-6Al-4V elongated to a tensile strain of 0.001% in a linear perturbation step. Even at very low strain the effect of void inclusions on the elastic modulus and the yield stress can be well understood. Comparison of the 2D and 3D stress distributions suggests a potential reason for the discrepancies observed in our large deformation simulations. Despite being of identical porosity, the 2D model is more sensitive to the effects of large voids and stress concentrators whereas the 3D model is afforded additional protection and stability by its additional shell walls.

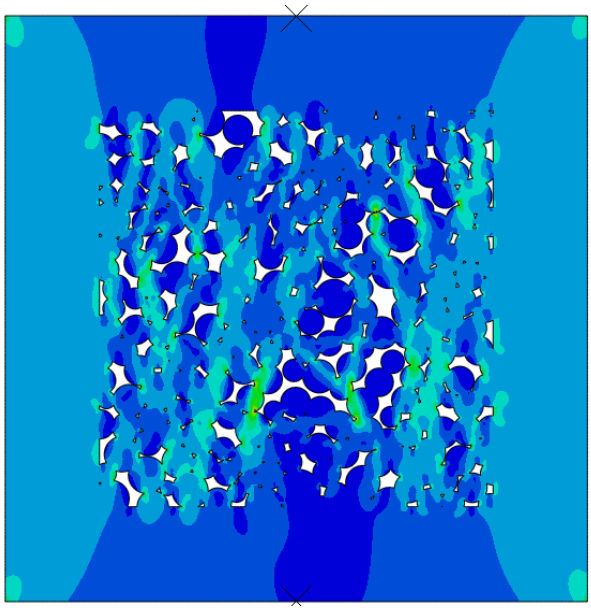

Figure 8. 2D Stress Plot - Elastic Tension

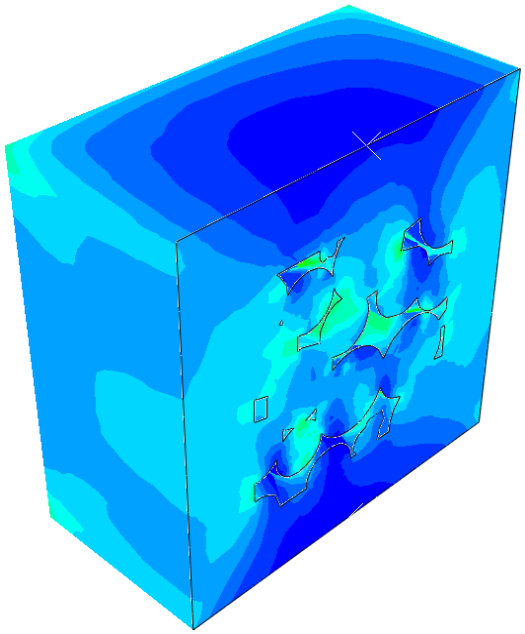

Figure 9. 3D Stress Plot - Elastic Tension

V. Conclusions

The particle generation and compaction algorithms presented in these works produce realistic geometric models that closely approximate the characteristics of sintered powder-based solids of a given porosity. The iterative particle arrangement process in particular mimics the particle settling phenomena more accurately than random particle placement.

The iterative compaction algorithm in concert with the analytical volume calculator have been proven to generate particle-based models of a specified porosity in an automated, precise, and efficient manner. Extensive testing of individual volume evaluation functions suggests that the discrepancies observed in the prediction of material elastic properties may be a result of discretization error inherent in the polygon-based measurement and analysis methods.

The tools developed by this work produce valuable predictions of mechanical behavior as a function of fractional porosity. The mechanical behavior observed from the finite element analysis of these RVEs predicts the experimental behavior of sintered metals more accurately than conventional porous RVE formulations.

Two dimensional porous RVE models are more susceptible to the effects of geometric stress concentrators than three dimensional models at large strains. Three dimensional RVE models should be used to model the large deformation behavior of porous materials, especially where sintered material porosity is in excess of 5%.

The findings of these simulations contribute significantly to our understanding of the effect of void shape, void size, and void fraction on the mechanical properties of porous metals. This tool is a viable source of experimental data where experimental data is not sufficiently available.

[1] H. H. Hausner, "The effect of porosity on the structure of sintered metals," *Journal of the Japan Society of Powder and Powder Metallurgy*, vol. 7, no. 2, pp. 58-72, 1960.

[2] K. Yamaguchi, N. Takakura and S. Imatani, "Compaction and sintering characteristics of composite metal powders," *Journal of Materials Processing Technology*, vol. 63, no. 1-3, pp. 364-369, 1997.

[3] L. Bertini, V. Fontanari and G. Straffelini, "Tensile and bending behavior of sintered alloys: experimental results and modeling," *Journal of Engineering Materials and Technology*, vol. 120, no. 3, pp. 248-255, 1998.

[4] C. T. Sun and R. S. Vaidya, "Prediction of composite properties from a representative volume element," *Composites Science and Technology*, vol. 56, no. 2, pp. 171-179, 1996.

[5] N. Chawla and X. Deng, "Microstructure and mechanical behaviour of porous sintered steels," *Materials Science and Engineering: A*, vol. 390, no. 1-2, pp. 98-112, 2005.

[6] R. J. Bourcier, D. A. Koss, R. E. Smelser and O. Richmond, "The influence of porosity on the deformation and fracture of alloys," *Acta Metallurgica*, vol. 34, no. 12, pp. 2443-2453, 1986.

[7] Dassault Systemes, *ABAQUS 6.14 Documentation*, Rhode Island, Providence, 2014.